ELSEVIER

Journal of Nuclear Materials 245 (1997) 131–137

journal of nuclear materials

A microstructural comparison of two nuclear-grade martensitic steels using small-angle neutron scattering

R. Coppola [a], F. Fiori [b], E.A. Little [c], M. Magnani [d,*]

[a] *ENEA, Casaccia, CP 2400, 00100 Rome, Italy*
[b] *Istituto di Scienze Fisiche, University of Ancona, Istituto Nazionale Fisica della Materia UdR Ancona, Ancona, Italy*
[c] *Department of Materials Engineering, University of Wales, Swansea SA2 8PP, UK*
[d] *ENEA, Clementel, V. Don Fiammelli 2, 40129 Bologna, Italy*

Received 26 November 1996; accepted 21 February 1997

Abstract

Results are presented of a small-angle neutron scattering (SANS) study on two 10–13% Cr martensitic stainless steels of interest for nuclear applications, viz. DIN 1.4914 (MANET specification, for fusion reactors) and AISI 410. The investigation has focussed principally on microstructural effects associated with the differences in chromium content between the two alloys. The size distribution functions determined from nuclear and magnetic SANS components for the two steels given identical heat treatments are in accord with an interpretation based on the presence of ~ 1 nm size C–Cr aggregates in the microstructure. Much larger (~ 10 nm) scattering inhomogeneities with different magnetic contrast are also present and tentatively identified as carbides.

1. Introduction

Ferritic-martensitic steels with 10–13% Cr have emerged as realistic options for structural components such as the 'first wall' in near-term fusion reactor devices, principally as a consequence of the low void swelling of these alloys under irradiation. A modified version of steel in this category, designated DIN 1.4914 (MANET), has been developed, initially as a potential candidate for the Next European Torus project and experimental programmes have been devised to characterize the material. General information on this steel and its microstructure can be found in Refs. [1–3], while Refs. [4,5] report more specifically results of transmission electron microscopy (TEM) observations. Other microstructural studies have included X-ray diffraction and small-angle neutron scattering (SANS) measurements [6–10]. SANS is a useful technique that enables small inhomogeneities such as clusters and precipitates in the size range around 1 nm to be resolved. An indication of precipitate type and composition can be obtained by analyzing magnetic and non-magnetic SANS components. An important aspect of the above SANS studies is the detection of C–Cr aggregates which give rise to SANS anisotropy and which are sensitive to heat treatment. In particular, it was reported [8–10] that MANET steel quenched from 1200°C exhibits isotropic SANS intensity much weaker than if quenched from lower temperatures; this is consistent with the prediction that the aggregates are unstable above 1180°C [8,9] and thus their absence following quenching from high temperatures results in the disappearance of the magnetic SANS anisotropy. The importance of these aggregates is that they may precede the formation of bcc α' precipitates (Cr-rich ferrite) [11–13] which are responsible for '475°C-embrittlement' characterized by marked ductile–brittle transition shifts. Such effects are well known in high Cr (> 18%) fully ferritic steels following long term thermal aging in the temperature range 350–500°C, but have also been observed in compositions down to ~ 13% Cr [13]; α' precipitation has also been detected in 10–13% Cr martensitic steels similar to those used in the present investigation, following fast reactor irradiations to 23 dpa [14]. It is

* Corresponding author. E-mail: magnani@risc990.bologna.enea.it.

PII S0022-3115(97)00019-6

also noted that long-range pseudo-periodic variations in Cr concentration have been observed in dual-beam irradiated MANET steel and characterized using atom probe/field ion microscopy [15]. These observations imply that Cr redistribution under irradiation may be important in controlling the overall irradiated microstructure.

In order to provide further insight into this phenomenon additional SANS studies have been undertaken on AISI 410, a martensitic steel with higher Cr content, using identical heat treatments. Intuitively it may be expected that increasing the Cr content should enhance the C–Cr clustering process and this should be apparent in the SANS spectra. The results of the measurements are presented and discussed in this paper.

2. Experimental

2.1. Materials

The MANET-type (heat 51482) samples were provided by Forschungs Zentrum, Karlsruhe (Germany). The chemical composition of this steel is as follows: C 0.17, **Cr 10.5**, Mo 0.5, Ni 0.85, Mn 0.60, Nb 0.20, V 0.25, Si 0.32, Al 0.005 and Fe to balance (wt%). The chemical composition of the AISI 410 steel is as follows: C 0.15, **Cr 13.0**, Ni 0.47, Si 0.30, P 0.021, S 0.027 and Fe to balance (wt%). Samples of the two materials suitable for SANS measurements were machined in the form of rectangular plates approximately $10 \times 5 \times 1$ mm^3 in size. For each material, two heat treatments were used: (i) austenitization at 1075°C for 0.5 h followed by quench ($T' = 150$°C/min); (ii) as for (i) but followed by tempering at 700°C for 20 h.

Furthermore, as reported previously [8–10] a MANET sample austenitized at 1200°C for 0.5 h and then quenched ($T' = 3600$°C/min) was also studied.

2.2. SANS technique

It is well known that small-angle neutron scattering (SANS) consists of the angular broadening around the primary direction, usually within $2\theta \leq 5°$, of a collimated monoenergetic neutron beam (neutron energy 25 meV or less) passing through a sample with chemical or magnetic inhomogeneities of size d, such that $Qd \ll 1$. Since typical neutron wavelengths range from $\lambda = 0.5$ to 1.5 nm approximately, 'small' values of the wave vector $Q = 4\pi(\sin\theta)/\lambda$ imply d values much larger than interatomic distances and correspond to inhomogeneities such as precipitates or microvoids. The use of neutron beams offers the key advantage that samples of bulk material, typically of ~ 1 mm thickness, can be readily characterized. Furthermore, since the interaction of neutrons with condensed matter depends on the neutron scattering length, which varies randomly from one element to another, elements of close atomic number (e.g., Fe and Cr) can easily be distinguished using the technique. Finally, owing to their magnetic spin moment, neutrons represent a unique probe for the study of bulk magnetic materials. Therefore SANS is an ideal technique to investigate microstructural processes in ferritic/martensitic steels subjected to thermal and mechanical treatments such as aging, creep and fatigue or to irradiation. A full description of the SANS technique and methods of data analysis are given in Ref. [6].

The SANS measurements were carried out using the PAXY instrument at Laboratoire Léon-Brillouin (CEA-CNRS, Saclay). The MANET and AISI 410 samples were measured in the course of two different SANS experiments using the same experimental conditions, namely a beam size of 8 mm diameter with a sample-to-detector distance of 2 m and a wavelength of 6 Å. This gave a Q-interval ranging from 0.02 to 0.16 Å^{-1}, which corresponds to particle sizes ranging from 1 to 5 nm approximately; the effect of scattering centres with size outside this interval (i.e., larger) may also be estimated, as shown below. A horizontal magnetic field of 1.4 T was applied perpendicular to the incident neutron beam (and in the plane of the sample surface) in order to fully align the magnetic moments in the sample. Thus only nuclear scattering occurs in the horizontal plane, while nuclear and magnetic scattering both occur in the vertical one. For the case of magnetic samples the total SANS cross-section $(\mathrm{d}\Sigma/\mathrm{d}\Omega)(Q)$ can be written as

$$\frac{\mathrm{d}\Sigma}{\mathrm{d}\Omega}(Q) = \left(\frac{\mathrm{d}\Sigma}{\mathrm{d}\Omega}(Q)\right)_{\mathrm{Nucl.}} + \left(\frac{\mathrm{d}\Sigma}{\mathrm{d}\Omega}(Q)\right)_{\mathrm{Mag.}} \sin^2\Phi, \quad (1)$$

where Φ is the azimuthal angle from the horizontal direction on the two-dimensional detector plane. The nuclear component is the horizontal one ($\Phi = 0°$), while the magnetic one is obtained as the difference between the vertical and the horizontal components. In practice the nuclear and magnetic SANS components are obtained by regroupment of the two-dimensional data selecting 15° wide opposite sectors of the area detector, horizontal for the nuclear component ($\Phi = 0°$) and vertical for the sum of the nuclear and of the magnetic one ($\Phi = 90°$), as shown in Ref. [9]. The ratio of the 'vertical' to the 'horizontal' SANS cross-sections

$$R(Q) = \frac{\left(\frac{\mathrm{d}\Sigma}{\mathrm{d}\Omega}(Q)\right)_{\mathrm{Nucl.}} + \left(\frac{\mathrm{d}\Sigma}{\mathrm{d}\Omega}(Q)\right)_{\mathrm{Mag.}}}{\left(\frac{\mathrm{d}\Sigma}{\mathrm{d}\Omega}(Q)\right)_{\mathrm{Nucl.}}} \quad (2)$$

is related to the composition of the microstructural defects. Its dependence on Q implies that defects of different size or composition contribute to different parts of the total SANS spectrum. The SANS nuclear and magnetic cross-sections can each be written as

$$\frac{\mathrm{d}\Sigma}{\mathrm{d}\Omega}(Q) = (\Delta\rho)^2 \int_0^{+\infty} N(R) V^2(R) |F(Q, R)|^2 \, \mathrm{d}R, \quad (3)$$

where $(\Delta\rho)^2$ is the neutron 'contrast', depending on the chemical composition of the scattering centres, $N(R)\,\mathrm{d}R$

is the number of centres with a typical size between R and $R + dR$, V their volume and $|F(Q, R)|^2$ their form factor (assumed spherical in the present study). $N(R)$ was determined using the method described in Refs. [16,17]. This code assumes that $N(R)$ can be written as a combination of a suitable number of cubic B-spline functions, with the constraint $N(R) > 0$ and gives an uncertainty band statistically determined by the quality of the best-fit. In fact Eq. (3) must be solved while the SANS cross-section is known only in a limited Q-interval. The method has up to now proved to be quite reliable, as shown, for instance, by the results reported in Ref. [4]. Also the SANS spectra, obtained with different wavelengths, of the same two MANET samples considered in this work, give closely comparable size distribution functions. Large uncertainty bands can originate from the evaluation of the high-Q background level, which is particularly relevant in the case of scattering centres as small as those investigated in this study.

A knowledge of the best-fit determined $N(R)$ gives the volume distribution function defined in this case as $D(R) = N(R) \cdot R^3$. From $N(R)$ it is also possible to obtain the average size and, provided the contrast factor is known, the volume fraction of the scattering centres. When, as in the present case, the composition of the scattering centres is not precisely determined only the relative values of the volume fraction can be compared for samples having the same $(\Delta\rho)^2$.

3. Results and discussion

Fig. 1(a) and (b) illustrate, respectively, the nuclear and magnetic SANS cross-sections determined for the samples investigated. The SANS cross-sections of the MANET sample quenched from 1200°C are also reported for comparison. Fig. 2 illustrates the $R(Q)$ ratios. The following general features are evident from the data:

— The SANS cross-sections of the samples quenched from 1075°C are much higher than those of the MANET sample quenched from 1200°C.

— The influence of the 20 h tempering treatment on the two materials is to increase the nuclear SANS intensity. At lower Q values, which correspond to larger particle sizes, this response can readily be interpreted as the growth of precipitates (probably carbides) as a consequence of tempering. The slopes of the SANS curves appear different from one material to another (especially the magnetic component of the two tempered samples) and this gives rise to differences in the size distribution functions presented below.

— The $R(Q)$ ratios of the two materials show a very similar behaviour, namely a dependence on Q, which is particularly marked in the as-quenched condition. As discussed for the case of MANET in Refs. [9,10], this implies the presence of microstructural inhomogeneities of different sizes and composition.

The comparison, for equal thermal treatment, between

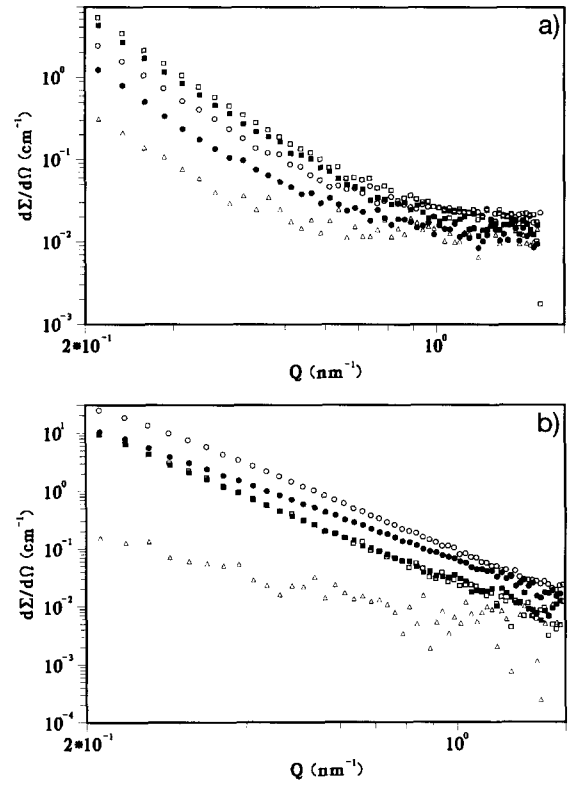

Fig. 1. (a) Nuclear and (b) magnetic SANS components for MANET (empty symbols) and for AISI 410, as-quenched condition (circles) and after 20 h at 700°C (squares). The nuclear and magnetic SANS cross section of the MANET sample quenched from 1200°C are also reported (triangles).

the two materials implies less evident considerations. Within the selected Q-range, the SANS intensities of AISI 410 are generally lower than those of MANET, though the points at higher Q-values (corresponding to the smallest scattering centres) should be considered with caution due to their wide fluctuations and to the fact that the samples of the two materials were measured in two separate experi-

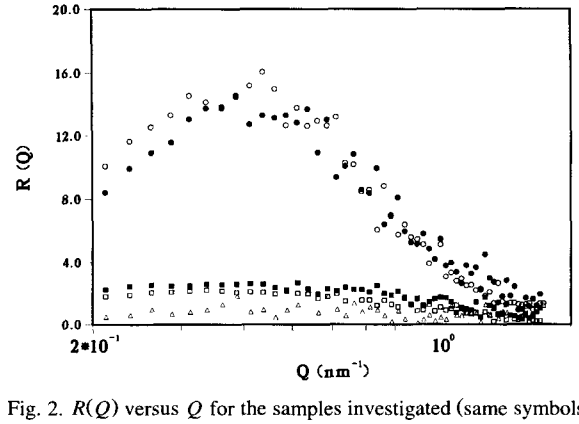

Fig. 2. $R(Q)$ versus Q for the samples investigated (same symbols as in Fig. 1).

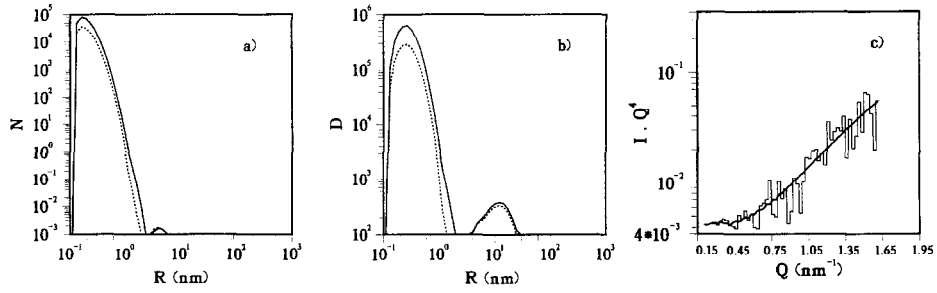

Fig. 3. As-quenched MANET sample: (a) size distribution function $N(R)$ (number of particles per unit volume with radius between R and $R + \mathrm{d}R$), (b) volume distribution function ($N(R) \cdot R^3$) and (c) check of the Porod-law (the continuous line represents the best-fit data) for the nuclear SANS component. The distribution functions obtained by subtracting the sample quenched from 1200°C are also reported (dotted line).

ments. This high Q-region contains SANS contributions arising from all the fine-scale microstructural features present in each of the two materials. In the case of MANET, it is assumed that the 'true' information pertaining to C–Cr aggregates can be obtained by subtraction of the sample quenched from 1200°C [10]. As no similar reference is available for AISI 410 (the critical quench temperature could in principle be different from that of MANET) in the following discussion the data from AISI 410 are compared to those of MANET without subtraction of this reference sample.

The size distribution function, $N(R)$, as defined in Eq. (3), was determined for the four samples using the published code [16,17] and calculated separately for the nuclear and the magnetic SANS components. Fig. 3(a) and (b) show, respectively, the size and volume distribution functions of the as-quenched MANET sample calculated from the nuclear component; there is a well-defined peak at an average radius of about 0.5 nm, with some considerably larger particles giving a significant contribution to the total volume fraction. As explained earlier this peak contains all the fine-scale contribution from the MANET matrix, including that arising from the C–Cr aggregates. Their contribution can be extracted by determining the distribution function of the same sample after subtraction of the sample quenched from 1200°C. The size distribution function obtained after this subtraction is reported for comparison in Fig. 3(a) and (b). Turning next to the magnetic component, as illustrated in Fig. 4(a) and (b), the peak at higher radius becomes predominant in the volume distribution and the size distribution functions are affected by a much larger uncertainty band (not reported in the picture). This is partly due to the greater statistical fluctuations (i.e., because the input spectra are obtained as the difference between two data sets), but also implies the presence of scattering centres in a size range completely outside the selected Q-region and much larger than the size dominating the nuclear component. This is confirmed by comparing the asymptotic behaviour predicted by the 'Porod law' (Q^{-4}) as given in Fig. 3(c) and Fig. 4(c) which demonstrates that this asymptotic behaviour (which can be observed for scattering centers having a minimum size $\gg 1/Q$, or at least some 10 nm in our case) is present only for the magnetic component, in agreement with Fig. 4(a) and (b). In contrast, the size of the scattering centres dominating the nuclear component is so small that the Porod region cannot be observed within the Q-interval. The nuclear and magnetic size distribution functions of the three other samples examined are qualitatively similar to those of Figs. 3 and 4 respectively, namely a population of large scattering centres appears in the magnetic component.

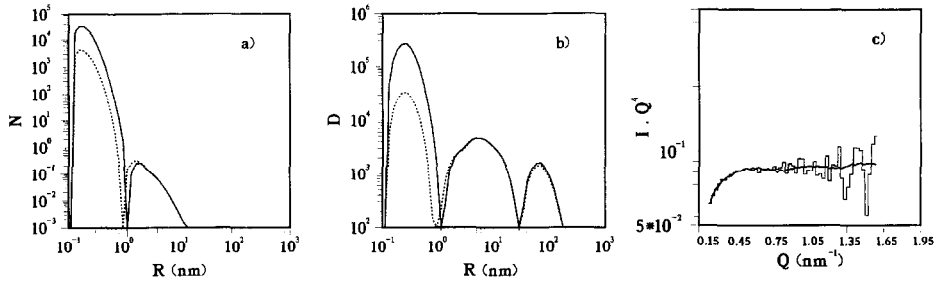

Fig. 4. As-quenched MANET sample: same caption as in Fig. 3, but for the magnetic SANS component.

The overall microstructural features of the 10–13% martensitic steels in terms of precipitated phases are well established, principally from electron microscope studies [14,18]. The major volume fraction of precipitates is generally $M_{23}C_6$ in all grades and this phase can incorporate Mo and V in steels containing such additions (e.g., DIN 1.4914). In Nb-containing grades, niobium carbide precipitates out separately. The carbides are generally in the size range above ~2 nm and extending to large sizes. They precipitate during tempering but will also coarsen during prolonged tempering. However, a carbide distribution is typically present in the as-quenched condition, representing both carbides undissolved or only partially dissolved by the austenitizing treatment together with limited precipitation processes occurring during the quench (viz. 'autotempering'). It follows that a reasonable interpretation of the calculated distribution functions, which have the same basic form in all the samples examined, is to attribute the peak present at large radii in Fig. 4(b) to non-magnetic precipitates (most likely $M_{23}C_6$), embedded in a strongly magnetic matrix and giving therefore a SANS contrast markedly different from that of the smaller scattering centres (C–Cr aggregates). In fact in Fig. 3(a) (nuclear component) the intensity of the secondary peak, determined by the product of the nuclear contrast and the volume fraction of such precipitates, is much lower than in the magnetic component. Sensitivity tests have been carried out by varying the input parameters of the size distribution function code, in order to establish more accurately the average radius and the 'intensity' of the main peak in Fig. 3(a) and for the other samples. Within a broad

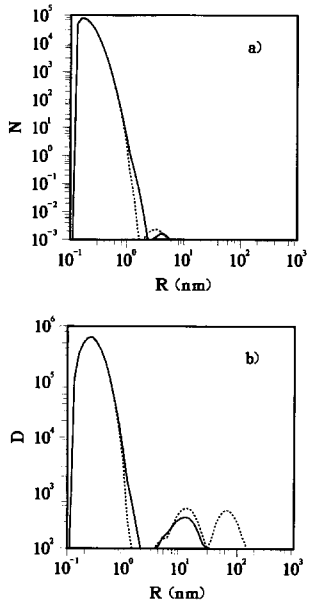

Fig. 5. (a) Size and (b) volume distribution functions for the nuclear SANS components of as-quenched (continuous line) and tempered (dotted line) MANET samples.

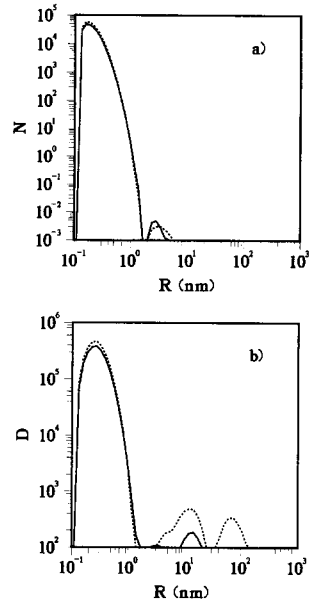

Fig. 6. (a) Size and (b) volume distribution functions for the nuclear SANS components of as-quenched (continuous line) and tempered (dotted line) AISI 410 samples.

range of input parameters such as number of *B*-splines and minimum radius value, the result of the fit is quite close to that reported in the data as presented, but the subtraction of an arbitrary background can strongly modify the intensity of the small size peak. The invariance of this result confirms that the peak contains genuine physical information on the finer microstructural features present in the materials. On the other hand, for such data it is difficult to resolve differences in the region of radius values less than 1 nm, which is typically regarded as the resolution limit for the SANS technique. Furthermore, with regard to the magnetic component in Fig. 4(a), the reliability is significantly less, due to the presence of a bimodal distribution with a large uncertainty band (30% or more).

Despite these quantitative limitations, the present data contain new and interesting metallurgical information on 10–13% Cr martensitic steels. These features are most readily appreciated by replotting the data for the as-quenched and tempered conditions on the same axes; as presented for MANET in Fig. 5 and for AISI 410 in Fig. 6. Similarly, comparison between trends in MANET and AISI 410 can be seen in detail by plotting data for the two steels on the same axes and these are given in Figs. 7 and 8 for as-quenched and tempered conditions respectively. For the sake of clarity, the statistical error bands are not reported in these data. For the nuclear distributions they are generally much smaller than 10%, as it is shown by the data published in Ref. [9] which refer to the same MANET samples. Considering first the MANET steel (Fig. 5(a) and (b)), it appears that, after 20 h tempering at 700°C, the increases in the number density or radius of small scatter-

ing centres having a size of a few nm (C–Cr aggregates) are smaller than the uncertainty band, which is ~ 2–3% in this case. A slight increase in radius after tempering 20 h at 700°C can be inferred from the data of Ref. [10] referring to the same two samples after subtraction of the sample quenched from 1200°C. The contribution to volume distribution appearing, after 20 h at 700°C, around 100 nm (Fig. 5b) can reasonably be attributed to the growth of large $M_{23}C_6$ precipitates. Turning next to the AISI 410 steel (Fig. 6(a) and (b)), the effect of tempering is to induce a noticeable increase in size distribution for the features with smaller radii. Noticeable also is a significant contribution to the volume distribution at large radii (100 nm) as seen in Fig. 6(b), and which can tentatively be attributed to an increased amount of carbide precipitates. This in entirely consistent with the known tempering behaviour of the martensitic steels as a function of alloy content [18]. In particular, steels that do not contain Mo and/or V additions, such as AISI 410, exhibit reduced resistance to tempering compared with more highly alloyed grades (e.g., DIN 1.4914), such that rapid growth and averaging of carbides occurs, typically at tempering temperatures of 700°C and above. Clear differences between the two types of steel, larger than the experimental uncertainty, are not apparent from a comparison of the nuclear size distribution functions for identical heat treatments, as presented in Figs. 7 and 8. The MANET steel shows a higher intensity (especially in the main peak) compared to the AISI 410 alloy for both as-quenched and tempered conditions, but as previously mentioned this refers to all the fine-scale microstructural features of the

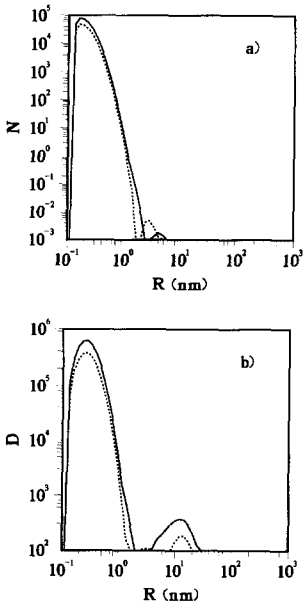

Fig. 7. (a) Size and (b) volume distribution functions for the nuclear SANS components of MANET (continuous line) and of AISI 410 (dotted line) as-quenched samples.

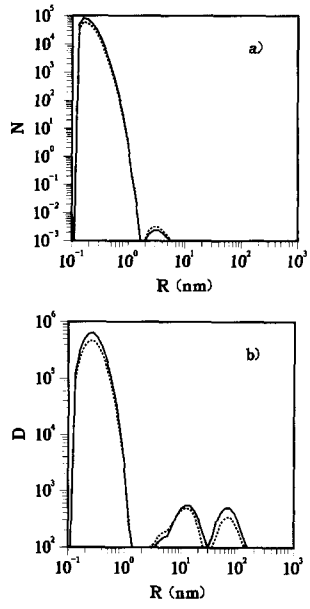

Fig. 8. (a) Size and volume (b) distribution functions for the nuclear SANS components of MANET (continuous line) and of AISI 410 (dotted line) tempered samples.

material. A slightly higher average radius in the AISI 410 steel may be inferred. A consistent increase in the radius of large particles in both steels as a consequence of tempering is also evident from the magnetic size distribution functions, despite large uncertainty bands which is in accord with an interpretation based on carbide precipitation at 700°C. The comparison between the magnetic components of the steels after 20 h tempering shows a much higher density of small scattering centres, which can also be inferred by the slope of the curves in Fig. 1(b). For large particles, SANS measurements at lower Q-values can be calibrated by reference to histograms of carbide size determined by electron microscopy, as discussed elsewhere [4]. At higher Q-values more detailed information can be deduced from small and wide angle polarized neutron scattering measurements and these have recently been carried out on MANET [19]. The preliminary data trends show nuclear and magnetic size distribution functions in excellent agreement with those of Figs. 3 and 4.

4. Conclusions

A SANS study has been undertaken to compare the fine-scale microstructural features of MANET (DIN 1.4914, fusion grade) and AISI 410 martensitic steels containing 10.5 and 13.0 wt% Cr, respectively. The principal conclusions emerging from an analysis of the size distribution functions and a comparison between nuclear and magnetic SANS components, are as follows:

(i) MANET and AISI 410 steels both contain a fine-scale microstructure consisting of an array of very small

inhomogeneities ~ 1 nm in size, and interpreted as C–Cr aggregates. Much larger features, with different magnetic contrast, are also present and tentatively identified as carbides.

(ii) The effect of tempering for 20 h at 700°C is to induce a small but detectable increase in the fine-scale scattering centres in both steels and particularly in AISI 410. The tempering also induces a marked increase in the density of larger size particles.

(iii) For equal thermal treatment the differences in the size distribution functions of the two steels are smaller than the experimental uncertainties; more detailed conclusions could be drawn by subtracting from the SANS data of each steel a reference sample, as for the case with the MANET sample quenched from 1200°C [10].

(iv) It is tentatively suggested that the formation of C–Cr clusters in martensitic steels after standard heat treatment may have important consequences in controlling Cr-rich ferrite (α') formation and/or Cr redistribution profiles in such alloys after high dose irradiation.

Acknowledgements

The support of the HCM Program for carrying out the SANS experiments is acknowledged. The authors are indebted to M. Ceretti and Dr A. Lapp (LLB, Saclay) for valuable collaboration.

References

[1] C. Wassilew, K. Herschbach, E. Materna-Morris, K. Ehrlich, Proc. Topical Conf. on Ferritic Alloys for Use in Nuclear Energy Technologies, Snowbird, UT (Metallurgical Society of AIME, 1983) p. 604.
[2] M. Schirra, Forschungs Zentrum Karlsruhe Report KFK (1984) p. 3640.
[3] R.L. Klueh, K. Ehrlich, F. Abe, J. Nucl. Mater. 191–194 (1992) 116.
[4] G. Albertini, F. Carsughi, R. Coppola, F. Rustichelli, W. Vlak, C. van Dijk, J. Nucl. Mater. 179-181 (1991) 706.
[5] D. Gavillet, P. Marmy, M. Victoria, J. Nucl. Mater. 191-194 (1992) 890.
[6] G. Albertini, R. Coppola, F. Rustichelli, Phys. Rep. 233 (1993) 137.
[7] R. Coppola, P. Lukas, R. Montanari, F. Rustichelli, M. Vrana, Mater. Lett. 22 (1995) 17.
[8] G. Albertini, M. Ceretti, R. Coppola, F. Fiori, P. Gondi, R. Montanari, Physica B212–214 (1995) 812.
[9] G. Albertini, F. Carsughi, R. Coppola, F. Fiori, F. Rustichelli, M. Stefanon, J. Nucl. Mater. 233–237 (1996) 253.
[10] R. Coppola, F. Fiori, M. Magnani, M. Stefanon, 1996. Invited talk at X SAS Conf., Campinas, J. Appl. Crystallogr., in press.
[11] I.A. Tomilin, V.I. Sarrak, N.A. Gorokhova, S.O. Suvorova, L.L. Zhukov, Fiz. Met. Metallogr. 56 (1983) 74.
[12] E.A. Little, D.A. Stow, Met. Sci. 14 (1980) 89.
[13] P.J. Grobner, Metall. Trans. 4 (1973) 25.
[14] E.A. Little, L.P. Stoter, ASTM STP No 782 (1982) 207.
[15] N. Wanderka, E. Camus, V. Naundorf, C. Keilonat, S. Welzel, H. Wollenberger, J. Nucl. Mater. 228 (1996) 77.
[16] M. Magnani, P. Puliti, M. Stefanon, Nucl. Instrum. Methods A271 (1988) 611.
[17] M. Stefanon, in: Proc. Int. School of Physics E. Fermi, Course CXIV on Industrial and Technological Application of Neutrons Lerici, June 1990, eds. M. Fontana, F. Rustichelli and R. Coppola (North Holland, Amsterdam, 1992) p. 113.
[18] E.A. Little, D.R. Harries, F.B. Pickering, S.R. Keown, Met. Technol. 4 (1977) 205.
[19] R. Kampmann, collaboration to be published.